Study of the Effect of Boron Concentration on Magnetic and Structural Properties of $Nd_{7.5}Pr_{2.5}Fe_{90-x}B_x$ Melt-Spun Alloys

M. Siddique[a,*], I. Ahmad[b], M. Kanwal[b] and E. Ahmed[a]
[a]Physics Division, PINSTECH, P.O. Nilore, Islamabad, Pakistan
[b]Department of Physics, B.Z. University, Multan, 60800, Pakistan

(Received March 28, 2013; in final form July 8, 2015)

The Mössbauer spectroscopy and X-ray diffraction techniques have been used to investigate the effect of boron concentration on the structural and magnetic properties of as-quenched and heat-treated melt-spun alloys $Nd_{7.5}Pr_{2.5}Fe_{90-x}B_x$ (x = 6, 8, 10) produced by melt-spinning technique. X-ray diffraction and Mössbauer spectroscopy results indicate that as-prepared samples are completely amorphous in nature. The X-ray diffraction patterns of samples heat-treated at 700 °C are indexed as Fe_3B, α-Fe, $(NdPr)_2Fe_{14}B$ and $Fe_{23}B_6$ phases. The Mössbauer spectra of heat-treated samples are very complex and constituted a number of sextets and a quadrupole doublet. Two main phases are $(NdPr)_2Fe_{14}B$ hard and t-Fe_3B soft magnetic phases while α-Fe and $Nd_{23}Fe_6$ are detected as minor phases. The average internal magnetic field decreases with the increase of boron content; more sharply in as-prepared and comparatively slowly in heat-treated samples. The X-ray diffraction and Mössbauer spectroscopy results are in good agreement with each other.

DOI: 10.12693/APhysPolA.128.353
PACS: 76.80.+y, 75.50.–y, 61.43.–j, 61.05.C–

1. Introduction

Nd–Fe–B permanent magnetic materials are very useful and well established having a number of applications in different devices like motors, generators, traveling wave tubes, and particle accelerators. These materials are based on $Nd_2Fe_{14}B$ hard phase which have large magnetization and high Curie temperature and thus have outstanding magnetic properties like intrinsic coercivity and energy product [1, 2].

The usefulness of rapid quenching technology to produce the high coercive Nd–Fe–B magnets reflects in the possibility to influence through the cooling rate directly on the grain size microstructure which can proved maximum magnetic energy of final magnetic materials [3-5]. The nanocrystalline magnetic materials based on Nd(Pr)–Fe–B alloys with low Nd content are new type of permanent magnetic materials. These materials are predominantly known as exchange-coupled nanocomposite hard magnetic materials having high remanence and magnetic energy despite reduce amount of expensive rare-earth Nd up to three times compared to classical permanent magnetic materials [6, 7]. The microstructure of these nanocomposites is a mixture of magnetically hard and soft phases like Fe_3B, Fe_2B, α-Fe and $Nd_2Fe_{14}B$. The presence of soft and hard phases in nanocomposites poses them to have large saturation magnetization and enhanced remanence [8].

These nanocomposites have some very important features: nanocrystalline grains whose size is of the order of a domain wall width, high iron content which generates high saturation magnetization and makes the magnet much less expensive, and a low rare-earth content which leads to a better corrosion resistant magnets [9]. Pinkerton and Dunham first report the Mössbauer spectrum of $Nd_2Fe_{14}B$ in both single phase ingot and melt-spun ribbon form. Spectra of melt-spun ribbon show the transformation from the magnetically soft Nd_2Fe_{17} phase in boron-free $Nd_{0.15}Fe_{0.85}$ alloy to the $Nd_2Fe_{14}B$ phase when 5 at.% boron is substituted for iron [10].

Magnetic nanocomposites containing hard phase in a soft matrix as $R_2Fe_{14}B/\alpha$-Fe, are promising materials for the production of resin-bonded magnets [11]. The Mössbauer spectroscopy is a very useful and powerful technique to find the particle size effect and the spin structure to study the supertransferred hyperfine interactions in magnetic materials. A Mössbauer spectrum can be characterized by the hyperfine parameters like internal magnetic field ($H_{\rm eff}$), quadrupole splitting (Δ) and isomer shift (δ). The effect of doping in magnetic materials can also be studied very effectively by the Mössbauer spectroscopy because the interactions can sense minute changes in the local crystalline structure and in the magnetic properties of the system [12–16]. In the present study we are presenting the effect of boron content and annealing on the magnetic properties of Nd(Pr)–Fe–B permanent magnetic materials.

2. Experimental

The ingots of alloys with nominal composition $Nd_{7.5}Pr_{2.5}Fe_{90-x}B_{6+x}$ (x = 6, 8, 10) were produced from individual elements having 99.99% purity using a laboratory scale argon-arc melting furnace with water cooled copper hearth. The weight of alloy for each melt

*corresponding author; e-mail: siddique56@hotmail.com

was 10 g. Initially chamber was rough evacuated and flushed with argon gas 4 to 5 times and then evacuated to less than 10^{-4} Torr prior to back filling with 1/3 atmospheric pressure of high purity argon gas. Titanium ingot was melted before the alloy melting to reduce the oxygen partial pressure. The ingot was broken into small pieces and washed with acetone to remove any oxides present and placed in a quartz crucible. The ingot was melted by rf induction heating at 6 kW and the melt was then ejected under an argon gas pressure onto the Cu wheel rotating at the speed of 30 m/s to produce over quenched ribbons. These ribbons were placed in quartz tubes. The tubes were evacuated to less than 10^{-4} Torr and back-filled with high purity argon gas to 1 atm and flushed 3 to 5 times to produce a very low oxygen atmosphere. The tubes were then refilled by argon gas at 1/3 atm of pressure. Each sample was heat treated in a preheated tube furnace at 700 °C for 10 min and then quenched in a water bath. X-ray diffraction studies were carried out on Rigaku X-ray diffractometer with Cu K_α radiation (1.5406 Å), 2θ ranges from 20° to 70°, step size of 0.02° and scanning speed of 1°/min. The magnetic properties of these ribbons were measured on a superconducting vibrating sample magnetometer with a maximum applied field of 9 T. The transmission electron microscopy (TEM) of these ribbons was performed at Philips 200 T. The Mössbauer measurements were carried out at room temperature using a ^{57}Co (Rh-matrix) source of initially 25 mCi strength, in transmission geometry. The Mössbauer spectrometer was calibrated using a thin α-Fe foil. The data analysis was performed using a computer program Mos-90 [17], assuming that all the peaks are Lorentzian in shape.

3. Results and discussion

XRD patterns of as-quenched samples are shown in Fig. 1, which are almost amorphous in nature, however, some singles can be noticed for the appearance of crystalline beaks at 2θ near 26 deg and 45 deg. This means that small amount of crystalline phase is going to develop at these points but not in the matured form. Whereas the samples annealed at 700 °C for 10 min are fully crystalline. In all the annealed samples four phases Fe_3B (tetragonal), α-Fe (cubic), $Nd_2Fe_{14}B$ (tetragonal) and $Fe_{23}B_6$ (cubic) coexists. All these phases matched very well with the JCPDS card # 39-1316, 06-0696, 80-0870 and 47-1332, respectively. XRD results of heat-treated samples also reveal that the most dominant peaks belonged to magnetically hard phase $(NdPr)_2Fe_{14}B$ along with magnetically soft phases Fe_3B, α-Fe and $Fe_{23}B_6$.

The morphology of grain distribution in annealed ribbons of all compositions is found very similar to one another. A typical transmission electron micrograph taken for $x = 10$ is shown in Fig. 2a. From this TEM micrograph it can be seen that grains are randomly oriented and are homogeneously distributed throughout the ribbons. In the inset in Fig. 2a, the broken halo

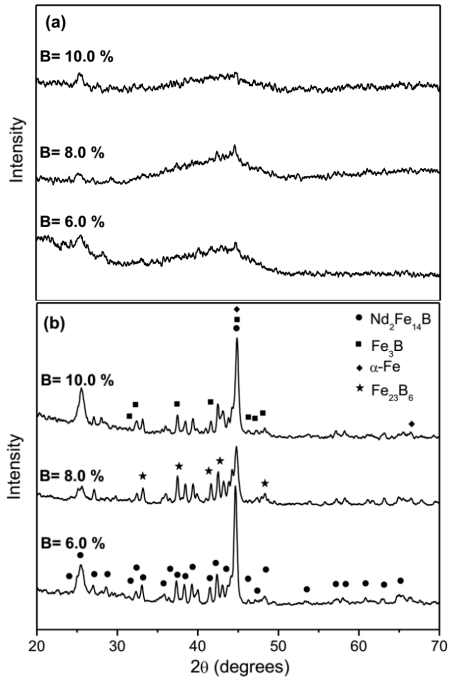

Fig. 1. XRD patterns of alloys $Nd_{7.5}Pr_{2.5}Fe_{90-x}B_x$ (a) as-prepared and (b) annealed samples at 700 °C for 10 min.

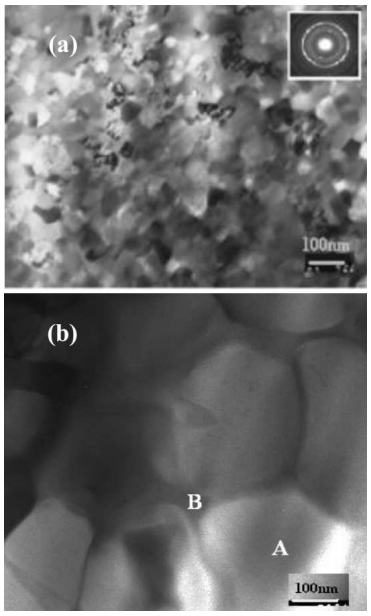

Fig. 2. (a) The morphology of grain distribution in annealed ribbons for $x = 10$, (b) selected coarser grain region showing hard (A) and soft (B) magnetic phases.

with dotted patterns indicates the combination of very small amorphous behavior along with these crystalline phases. In Fig. 2b, a selected coarser grain region is also shown and two different phases observed are marked as: (A) hard magnetic phase and (B) soft magnetic phase. The details are given in another publication of some of the authors of present study [18].

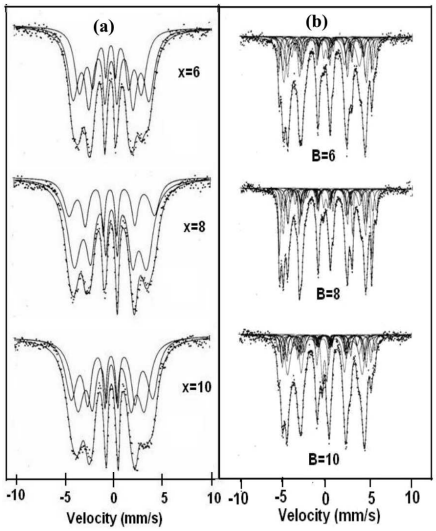

Fig. 3. Mössbauer spectra of $Nd_{7.5}Pr_{2.5}Fe_{90-x}B_x$ alloys, (a) as-prepared and (b) annealed samples at 700 °C for 10 min.

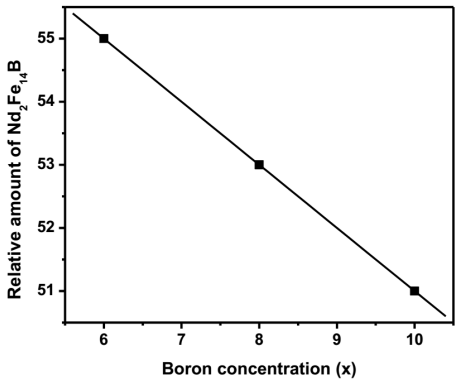

Fig. 4. Variation of $(NdPr)_2Fe_{14}B$ hard magnetic phase with B content in annealed $Nd_{7.5}Pr_{2.5}Fe_{90-x}B_x$ melt-spun alloys at 700 °C for 10 min.

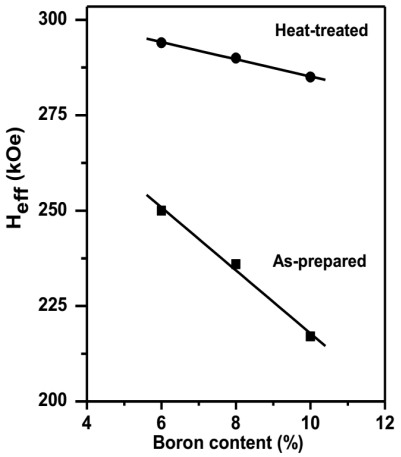

Fig. 5. Variation of average internal magnetic field with B content.

TABLE I

Mössbauer parameters of $Nd_{7.5}Pr_{2.5}Fe_{84-x}B_{6+x}$ ($x = 6, 8, 10$) melt-spun amorphous alloys.

Boron	H_{eff}	Δ	δ	Γ	Area
[%]	[kOe]	[mm/s]	[mm/s]	[mm/s]	[%]
6	239	0.00	−0.03	1.28	60
	195	−0.03	−0.09	1.20	40
8	260	0.06	−0.03	1.14	48
	212	−0.06	−0.09	1.52	52
10	270	0.05	0.18	1.24	30
	229	−0.12	−0.04	1.66	70

The Mössbauer spectra of as-quenched $Nd_{7.5}Pr_{2.5}Fe_{84-x}B_{6+x}$ ($x = 0, 2, 4$) alloys have been shown in Fig. 3a and their parameters are as summarized in Table I. The spectra of these samples show the characteristic features of amorphous materials, which are quite broad due to hyperfine field distribution. Each spectrum is well fitted with two magnetic sextets having very broad line widths indicating the amorphous nature of both iron sites. The immature crystalline peaks observed in XRD patterns of these alloys do not confirm the presence of any crystalline phase by the Mossbauer results. The average internal magnetic field increases with the increase of boron content as shown in Fig. 4. The Mössbauer spectra of annealed samples are shown in Fig. 3b. These spectra have very complex structure and contain a large number of components (subspectra) representing each iron site according to its environment. It is very difficult to fit such a complex spectra, however, with our past experience on these materials [19] we have succeeded to analyze these spectra. After a number of trials suitable fitting has been obtained. Ten magnetic sextets and one quadrupole doublet have been fitted in all samples. There are two main phases, $(NdPr)_2Fe_{14}B$ and t-Fe_3B, and two minor phases α-Fe and a paramagnetic phase probably $Fe_{23}B_6$ [20–22]. The appearance of a small amount of non-magnetic boride phase is due to the fact that all samples contain equal or greater than 6 at.% boron content [22]. More than 50% contribution is due to $(NdPr)_2Fe_{14}B$ phase in each sample. It has tetragonal crystal structure [23–26] in which iron occupies six sites and one for boron and two for rare earth elements, Nd and Pr. The six iron sites are $8j_1$, $8j_2$, $16k_1$, $16k_2$, 4c, and 4e. The assignment of these sites is based on the number of Fe atom as nearest neighbours and the fact that rare earth and boron atoms tend to decrease the magnetic moment of neighbouring Fe atoms. Different authors have used different criteria to assign these sites however we have used the scheme of Fruchart et al. [27] i.e. $H_{\text{hf}}(8j_1) > H_{\text{hf}}(4e) > H_{\text{hf}}(16k_1) > H_{\text{hf}}(16k_2) > H_{\text{hf}}(4c) > H_{\text{hf}}(8j_2)$. The amount of this phase increases with the increase of boron content, shown in Fig. 4. The α-Fe phase has different amount in all samples. The isomer shift values of all sextets are small and

close to electronic configuration of the iron atoms in the metallic iron. The average magnetic field of as-cast melt-spun ribbons decreases slowly, whereas it decreases more rapidly in heat-treated samples as shown in Fig. 5. In the Fe–B based amorphous or crystalline alloys B atoms occupy the central place of trigonal prism constituted by the Fe nearest atoms. If some fluctuations exist in the nearest-neighbour of B atoms, they bound to influence the electronic structure of B atoms, and consequently, change the hyperfine field and its distribution at B sites [28]. This indicates that boron atom lowers the internal magnetic field of the system in agreement with one of our earlier study [29]. Details of the Mössbauer parameters of annealed samples are given in Table II.

TABLE II

Mössbauer parameters of $Nd_{7.5}Pr_{2.5}Fe_{84-x}B_{6+x}$ ($x = 6, 8, 10$) melt-spun alloys annealed at 700 °C; bold parameters are of α-Fe and bold italic are parameters are of t-Fe_3B.

Boron	H_{eff}	Δ	δ	Γ	Area
[%]	[kOe]	[mm/s]	[mm/s]	[mm/s]	[%]
	346	0.6	-0.01	0.3	8
	334	**0**	**−0.13**	**0.21**	**6**
	324	0.2	0.19	0.35	10
	298	0.19	-0.13.	0.56	21
	281	**0.24**	**0**	**0.4**	**14**
6	272	0.2	-0.12	0.35	3
	270	-0.09	0.21	0.33	5
	262	**−0.04**	**−0.26**	**0.78**	**19**
	258	0.28	0.09	0.48	8
	230	**0.25**	**0.21**	**0.35**	**3**
	—	0.49	0.03	0.35	3
	346	0.67	-0.02	0.3	8
	333	**−0.01**	**−0.12**	**0.3**	**18**
	323	0.22	0.16	0.35	8
	299	0.08	-0.2	0.35	17
	288	**0.28**	**0.02**	**0.32**	**12**
8	281	0.12	0.34	0.27	4
	275	0.29	-0.07	0.4	14
	269	**−0.29**	**−0.24**	**0.58**	**10**
	253	0.42	-0.07	0.25	2
	232	**0.31**	**0.21**	**0.3**	**4**
	—	0.52	0.02	0.35	3
	351	0.65	0.1	0.3	07
	336	**0.28**	**−0.11**	0.55	**8**
	322	0.15	0	0.35	9
	302	0.26	-0.16	0.34	10
	293	**0.12**	**−0.1**	**0.35**	**7**
10	284	0.02	-0.08	0.4	8
	277	0.22	-0.05	0.35	8
	270	**0.23**	**−0.1**	**0.73**	**25**
	249	0	0	0.57	9
	225	**0.17**	**0**	**0.35**	**3**
	—	0.54	0	0.35	6

4. Conclusions

XRD results indicate that as-prepared samples are amorphous with some indication of small crystalline phase, whereas annealed samples are fully crystalline. Both studies reveal that annealed samples contain $(NdPr)_2Fe_{14}B$ and t-Fe_3B, $Fe_{23}B_6$ and α-Fe phases with some quantitative variation. The Mössbauer spectroscopy results also show that the average internal magnetic field of as-cast melt-spun ribbons decreases slowly, whereas, it decreases more rapidly in heat-treated samples with the increase of boron content. TEM micrograph shows that grains are round shape, randomly oriented and are homogeneously distributed throughout the ribbons. A selected coarser grain region shows the presence of two different phases: a hard magnetic phase and a soft magnetic phase.

Acknowledgments

Authors are thankful to Mr. M. Shafi and Mr. M. Talha for Mössbauer data collection.

References

[1] N.C. Koon, B.N. Das, *J. Appl. Phys.* **55**, 2063 (1884).

[2] M. Sagawa, S. Fujimura, N. Togawa, H. Yamamoto, Y. Matsuura, *J. Appl. Phys.* **55**, 2083 (1884).

[3] N. Talijan, J. Stajic-Trosic, A. Milutinovic-Nikolic, D. Minic, Z. Jovanovic, in: *Proc. V Int. Conf. on Fundamental and Applied Aspects of Physical Chemistry*, Eds. A. Antić-Jovanović and S. Anić, Society of Physical Chemists of Serbia, Belgrade 2000, p. 408.

[4] S.V. Andreev, N.V. Kudrevatykh, A.I. Kozlov, P.E. Markin, V.I. Pushkarsky, in: *Proc. XV Int. Workshop on Rare Earth Magnets, Dresden (Germany)*,Mat Info/Werkstoff-Informationsgesellschaft, Frankfurt 1998, Vol. 1, p. 119.

[5] V.P. Menushenkov, S.J. Andersen, R. Hoier, in: *Proc. XV Int. Workshop on Rare Earth Magnets, Dresden (Germany)*, Eds. L. Schultz, K.-H. Müller, Mat Info/Werkstoff-Informationsgesellschaft, Frankfurt 1998, Vol. 3, p. 97.

[6] R. Coehoorn, D.B. de Mooij, J.P.W. Duchateau, K.H.J. Buschow, *J. Phys. (France)* **C8**, 669 (1988).

[7] N. Talijan, J. Stajic-Trošic, A. Grujic, V. Cosovic, V. Menushenkov, R. Aleksic, *J. Min. Metal.* **41B**, 95 (2005).

[8] A. Manaf, R.A. Buckley, H.A. Davies, M. Leonowicz, *J. Magn. Magn. Mater.* **101**, 360 (1991).

[9] R.K. Murakami, V. Villas-Boas, *Mater. Res.* **2**, 67 (1999).

[10] F.E. Pinkerton, W.R. Dunham, *Appl. Phys. Lett.* **45**, 1248 (1984).

[11] R.K. Murakami, H.R. Rechenberg, A.C. Neiva, F.P. Missell, V. Villas-Boas, *J. Magn. Magn. Mater.* **320**, e65 (2008).

[12] G. Große, *MOS-90, Version 2.2 Manual and Program Documentation*, 2nd ed., March 1992.

[13] M.T. Sanchez, *J. Mater. Sci. Lett.* **15**, 461 (1996).

[14] A. Lehlooh, S. Mahmood, I. Abu-Aljarayesh, *J. Magn. Magn. Mater.* **136**, 143 (1994).

[15] J.S. Forrester, G.B. Schaffer, *Met. Trans. A* **26**, 725 (1995).

[16] M.F. Hansen, C.B. Hoch, S. Mørup, *Phys. Rev. B* **62**, 1124 (2000).

[17] C. Frandsen, S. Mørup, *J. Magn. Magn. Mater.* **266**, 36 (2003).

[18] I. Ahmad, H.A. Davies, M. Kanwal, *J. Magn. Magn. Mater.* **324**, 3971 (2012).

[19] M. Siddique, I. Hussain, I. Ahmad, N.M. Butt, *J. Radioanal. Nucl. Chem.* **261**, 151 (2004).

[20] M. Spyra, M. Leonowicz, *J. Magn. Magn. Mater.* **320**, e46 (2008).

[21] C. Zhao-hua, S. Bao-gen, Z. Jun-xian, M. Ming-xi, S. Ji-jun, Y. Chun-li, L. Fa-shen, Z. Yi-de, *Chin. Phys. Lett.* **14**, 387 (1997).

[22] A. Grujic, T. Zak, V. Cosovic, J. Stajic-Trosic, V. Spasojevic, N. Talijan, *Optoelectron. Adv. Mat. Rapid Commun.* **3**, 477 (2009).

[23] J.M. Friedt, A. Vasquez, J.P. Sanchez, P.L. Heritier, R. Fruchart, *J. Phys. F Met. Phys.* **16**, 651 (1986).

[24] D. Givord, J.M. Moreau, P. Tenaud, *Solid State Commun.* **55**, 303 (1985).

[25] P.C.M. Gubbens, A.M. van der Kraan, K.H.J. Buschow, *Phys. Status Solidi B* **130**, 575 (1985).

[26] A. Kostikas, V. Papaefthymiou, A. Simopoulos, G.C. Hadjipanayis, *J. Phys. F Met. Phys.* **15**, 129 (1985).

[27] R. Fruchart, P. L'Heritier, P. Dalmas de Reotier, D. Fruchart, P. Wolfers, J.M.D. Coey, L.P. Ferreira, R. Guillen, P. Vulliet, A. Yaouanc, *J. Phys. F Met. Phys.* **17**, 483 (1987).

[28] Z.H. Cheng, M.X. Mao, C.L. Yang, Y.D. Zhang, F.S. Li, B.G. Shen, J.X. Jhang, Ji-jun Sun, Yi-de Zhang, Fa-shen Li, *Phys. Rev. B* **52**, 9427 (1995).

[29] M. Arshed, M. Siddique, M. Anwar-ul-Islam, A. Ashfaq, A. Shamim, N.M. Butt, *Solid State Commun.* **98**, 427 (1996).